TRENDS IN SCIENCES 2025; 22(11): 10611
https://doi.org/10.48048/tis.2025.10611 RESEARCH ARTICLE

Highly Sensitive Electrochemical Sensor Modified with Pt/Pd-MnO_2/CNT Nanocomposite for the Determination of Glutamate

Chim Math[1], Paweenar Duenchay[2] and Wijitar Dungchai[1,*]

[1]Department of Chemistry, Faculty of Science, King Mongkut University of Technology Thonburi, Bangkok 10140, Thailand
[2]Department of Industrial Engineering, Manufacturing Engineering, and Chemical Processes and Environment Engineering, Faculty of Engineering, Pathumwan Institute of Technology, Bangkok 10330, Thailand

([*]Corresponding author's e-mail: wijitar.dun@kmutt.ac.th)

Received: 9 May 2025, Revised: 23 May 2025, Accepted: 10 June 2025, Published: 5 August 2025

Abstract

A novel nanocomposite comprising platinum/palladium-decorated manganese dioxide on carbon nanotubes (Pt/Pd-MnO_2/CNT) was successfully synthesized and immobilized onto a screen-printed carbon electrode (SPCE) for the electrochemical detection of glutamate. The electrocatalytic performance of the modified electrode was systematically evaluated using cyclic voltammetry (CV) and chronoamperometry (CA). Conventional glutamate biosensors that rely on the immobilization of glutamate oxidase often encounter several limitations, including high detection limits, electrode fouling, and poor operational stability, primarily due to enzyme leaching or denaturation. In contrast, the proposed sensor circumvents the need for enzyme immobilization on electrode by utilizing an electrocatalytic approach. This strategy maintains a high degree of analyte selectivity while significantly improving the sensor's stability, reproducibility, and overall analytical performance. The resulting sensor exhibited high sensitivity, with a detection limit of 1.98 µM, surpassing previously reported values. It demonstrated a linear response in the range of 0.005 - 0.08 mM and showed excellent selectivity by minimizing interference from common electroactive species such as ascorbic acid (AA) and uric acid (UA), thanks to a reduction-based detection mechanism. The sensor also exhibited strong durability, retaining 96 % of its initial signal after 3 weeks of storage. Furthermore, it demonstrated excellent repeatability and reproducibility, as well as high resistance to common interferences. Validation studies conducted on spiked samples showed recovery rates between 99 and 105 %, confirming the method's precision and accuracy. The practical application of the sensor was demonstrated through the quantification of glutamate in various instant noodle seasoning samples. The amounts of glutamate detected were 63.55 mg in Shrimp Tom Yum, 127.23 mg in Yentafo Tom Yum Mohfai, and 82.91 mg in Shrimp Creamy Tom Yum seasoning packets, respectively. In summary, the Pt/Pd-MnO_2/CNT-modified electrode offers a reliable, sensitive, and selective platform for real-time electrochemical detection of glutamate in complex food matrices, highlighting its potential for application in food safety and quality control.

Keywords: MnO_2/CNT, Nanomaterials, Glutamate quantification, Electrochemical sensor, Instant noodles

Introduction

L-glutamate, a naturally occurring amino acid, is widely utilized as a nutrient and flavor enhancer in various food products, including protein-rich plants such as rice and wheat, dairy products, meat, fish, eggs, and certain vegetables [1,2]. China dominates global production, accounting for approximately 80 % of total output, which has reached around 2.20 million tons annually in recent years [3]. Despite its extensive use and recognition as safe, concerns about its potential health effects persist. Excessive intake of L-glutamate has been associated with adverse symptoms. A 1995 FASEB report highlighted that individuals who consumed an oral placebo containing 0.5 - 2.54 g of L-glutamate experienced symptoms of Chinese Restaurant

Syndrome, including headaches and stomach discomfort, within 1 - 2 h [4,5]. Additionally, as the primary neurotransmitter in the brain, glutamate plays a crucial role in neuron communication and regulates learning and memory processes. Imbalances or dysfunctions in glutamate levels have been linked to various neurodegenerative disorders. High levels of L-glutamate can lead to excitotoxic damage and synaptic dysfunction, resulting in conditions like anxiety, depression, migraines/headaches, and pain. Conversely, insufficient levels can cause physiological dysfunctions such as lathyrism, amyotrophic lateral sclerosis, and Alzheimer's disease [6]. Therefore, accurate quantification of glutamate in food ensures food safety. In June 2017, the European Food Safety Authority (EFSA) reassessed the safety of glutamic acid and its inorganic salt forms, establishing a population-acceptable daily intake (ADI) of 30 mg per kg of body weight (b_w) per day (30 mg/kg b_w/day) [7]. Instant noodles are a globally popular food, widely consumed due to their convenience, affordability, and appealing flavors, making them a preferred choice for many, including children. According to the 2021 World Instant Noodles Association report, global consumption reached 116.5 billion servings, averaging 319 million daily servings [8]. Instant noodles are particularly popular in Asian countries, with the highest consumption recorded in China, followed by Indonesia, Vietnam, Japan, India, Thailand, and Malaysia [9]. The rising sales of affordable food options, such as instant noodles, have been linked to economic hardship, highlighting their role as a cost-effective dietary staple [10]. However, despite their widespread popularity, instant noodles have faced criticism for their high monosodium glutamate (MSG) content, raising concerns regarding potential adverse health effects.

Various analytical techniques have been reported for glutamate quantification, including chromatographic [11-13], spectrophotometric [14,15], capillary electrophoresis [16], and fluorescent-based methods [17]. However, these techniques often present significant drawbacks, such as large volumes of toxic solvents, rendering them non-ecofriendly, high costs and time-consuming procedures due to complex sample preparation and instrument operation. Electrochemical sensors offer a promising alternative, addressing these limitations with advantages such as simplicity, high sensitivity, reliability, portability, rapid response, and cost-effectiveness [18,19]. Electrochemically active materials play a crucial role in enhancing the performance of electrochemical techniques. Manganese dioxide (MnO_2), a transition metal oxide, exhibits significant electrocatalytic activity, chemical stability, affordability, and non-toxicity, making it highly efficient for detecting various analytes, including H_2O_2 [20]. However, its low electrical conductivity presents a limitation. To address this, MnO_2 is often combined with highly conductive carbon-based materials such as carbon nanotubes (CNTs) and graphene oxide (GO) to create advanced sensing materials with improved performance [21,22]. In addition to these materials, noble metal nanomaterials such as palladium (Pd) and platinum (Pt) have been widely utilized in electrochemical sensing due to their large surface area, high conductivity, and superior catalytic activity [23-25]. Among them, Pt stands out for its exceptional electrical conductivity and electrocatalytic properties, making it a highly attractive material for sensor development. However, its high cost, driven by limited natural abundance, has motivated extensive research to minimize Pt usage while maintaining its electrocatalytic efficiency [26]. One effective strategy involves alloying Pt with more cost-effective transition metals such as Pd [27], Cu [28] and Ni [29]which exhibits intense catalytic activity. Pt-M bimetallic catalysts offer reduced costs and enhanced catalytic activity and stability compared to monometallic Pt/C catalysts, owing to the synergistic interactions between the constituent metals. Notably, Pt-based alloy catalysts - especially those incorporating Pd - have garnered significant research interest due to their superior performance [30,31]. Additionally, the incorporation of metal oxides such as CeO_2 [32], CoO [33], and MnO_2 [34] , as well as deposition onto support materials like CNTs, further enhances electrocatalytic performance while reducing overall Pt consumption.

Various approaches have been employed in recent years to develop enzymatic biosensors for glutamate detection, primarily through immobilizing glutamate oxidase (GluOx) on different electrode surfaces. Several immobilization strategies have been reported, including direct immobilization of GluOx on electrode [35], co-immobilization of glutamate dehydrogenase (GLDH) and NAD^+ with multiwalled carbon nanotubes (MWCNTs) on a screen-printed carbon electrode [36],

and crosslinking GluOx with glutaraldehyde on a Prussian Blue modified electrode [37]. Another method involves immobilizing GluOx on a platinum nanoparticle-decorated MWCNT/polypyrrole (PPy) composite on glassy carbon electrodes (GC/Pt-MWCNTs/PPy/GluOx) [18]. Additionally, GluOx has been co-crosslinked with glutaraldehyde and chitosan on screen-printed electrodes [4,38,39]. However, these sensors typically suffer from high operational potentials and susceptibility to interference, limiting their applicability in complex sample matrices. To address these issues, low-operating detection potential sensors have been developed, including GluOx immobilized in a hydrophilic redox-silent polymer atop a horseradish peroxidase (HRP)/redox polymer-modified carbon nanoelectrode [40], GluOx immobilized on porous Co_3O_4 nanocubes for direct screen-printing (GluOx-Co_3O_4 nanocubes/SPE) [41], and an oriented immobilization strategy using a chitin-binding domain (ChBD-tag) on a screen-printed Prussian Blue nanocube microchip (ChBD-GluOxPB/SPC) [3].

Although previously developed enzymatic glutamate biosensors provide specificity through immobilized glutamate oxidase, they often suffer from high detection limits, electrode fouling, and reduced operational stability due to enzyme leaching or denaturation. Enzyme immobilization - typically achieved by directly coating the enzyme onto the electrode surface - can result in molecular adsorption, diminished electrocatalytic activity, and a shortened sensor lifespan. To overcome these limitations, we developed a hybrid enzymatic-electrochemical sensor that decouples enzyme activity from the electrode interface. As illustrated in **Schematic 1**, L-glutamate oxidase is introduced in solution to catalyze the oxidation of glutamate, producing H_2O_2, which is subsequently detected by a screen-printed carbon electrode (SPCE) modified with Pt/Pd-MnO_2/CNT nanomaterials. This configuration eliminates the need for enzyme immobilization while preserving enzymatic selectivity and significantly enhancing stability and reproducibility. The nanocomposite-modified electrode exhibits strong electrocatalytic activity toward H_2O_2 reduction, enabling sensitive detection with a low detection limit of 1.98 µM, a broad linear range (0.005 - 0.08 mM), and excellent stability (96 % retention after 3 weeks). Compared to conventional enzymatic sensors, this approach offers superior anti-interference capability and extended operational lifespan, making it particularly well-suited for glutamate quantification in complex food matrices such as instant noodle seasonings.

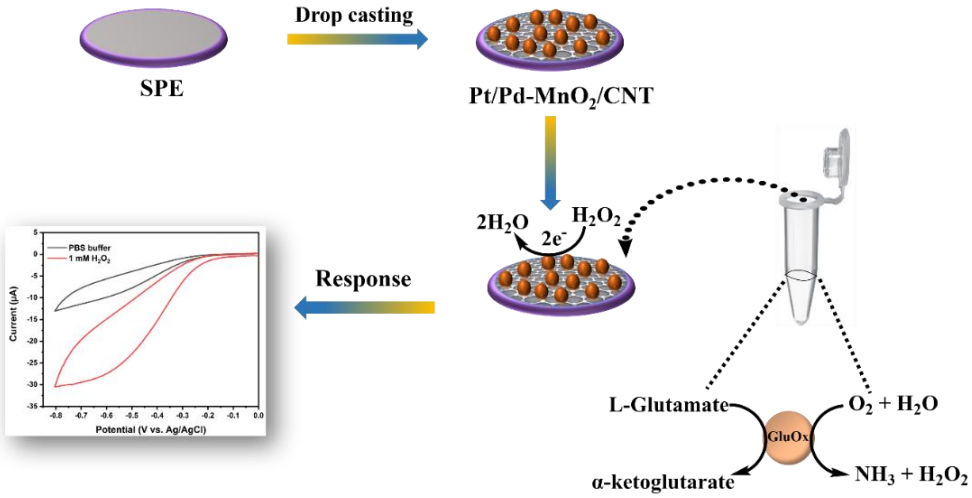

Schematic 1 Illustration of electrochemical detection of H_2O_2 on Pt/Pd-MnO_2/CNT.

Materials and methods

Chemical

Glutamic acid ($C_5H_9NO_4$) was bought from Ajax Finechem. Glutamate oxidase (recombinant, expressed in E. coli, lyophilized powder, ≥ 5.0 units/mg solid) and d-glucose ($C_6H_{12}O_6$) were purchased from Sigma Aldrich. Ascorbic acid ($C_6H_8O_6$) was bought from Loba Chemi. Palladium standard solution in 0.5 M HNO_3 ($Pd(NO_3)_2$, AAS standard), hydrogen peroxide (H_2O_2, 30 % w/w), potassium hexachloroplatinate (IV)

(K_2PtCl_6), and sodium hydroxide (NaOH) were obtained from Merck. Potassium dihydrogen phosphate (KH_2PO_4) was purchased from Qrëc. Potassium permanganate (VII) ($KMnO_4$), potassium chloride (KCl), sodium chloride (NaCl), sodium hydrogen phosphate (Na_2HPO_4), and D(-)-fructose ($C_6H_{12}O_6$) were brought from Kemau. Sucrose ($C_{12}H_{22}O_{11}$) was bought from Univar. Whatman filter paper no. 1 was purchased from Cytiva, USA. All reagents are analytical (AR) grade, and the PBS buffer (pH 7.4) was used as solvent throughout the experiment.

Instruments and apparatus

Cyclic voltammetry (CV) and chronoamperometry (CA) experiments were performed using an EmStat3 potentiostat with PSTrace 5.5 software from PalmSens. The study employed screen-printed carbon electrodes (SPEs) with the code CI1703OR, obtained from Quasense, Thailand. These SPEs consisted of a reference electrode (silver/silver chloride ink), an auxiliary electrode (carbon ink), and a working electrode (carbon ink with a 3 mm diameter), all supported by polycarbonate. The synthesized materials, including CNT, MnO_2/CNT, Pt/MnO_2/CNT, Pd/MnO_2/CNT, and Pt/Pd-MnO_2/CNT, were characterized using various advanced techniques. The morphology of the prepared electrodes was analyzed using scanning electron microscopy (SEM) (JEOL JSM-IT700HR). Additionally, transmission electron microscopy (TEM) (Talos F200X) was employed to measure the particle sizes of the nanocomposites.

Synthesis of nanomaterials

MnO_2/CNT

MnO_2/CNT was synthesized by a modified method [42]. Briefly, 50 mg of activated CNT was dispersed in 50 mL of 0.15 M $KMnO_4$ solution. The mixture was then sonicated for 30 min. Then, 5 mL of acetic acid was added while stirring at room temperature. Then, the solution was stirred at 70 °C for 2 h in an oil bath. Finally, the mixture was cleaned with deionized water (DI) by centrifugation to remove unreacted $KMnO_4$ and byproducts. Then, it was heated in the oven at 60 °C overnight.

Pd-MnO_2/CNT

To synthesize Pd-MnO_2/CNT, 60 mg of the synthesized MnO_2/CNT was mixed with 15 mL of deionized water. The mixture was then sonicated for 30 min to ensure proper dispersion. After that, 4 mL of a Pd standard solution (1,000 mg/L) was introduced into the mixture. The pH of the solution was adjusted to approximately 11 using 5 M NaOH, followed by adding 1 mL of a 0.5 M ascorbic acid (AA) solution. The AA solution acts as a reducing agent, converting Pd^{2+} to Pd^0 [43]. The solution was stirred at room temperature overnight. The next day, the mixture was purified using DI water through centrifugation and then heated at 60 °C in an oven overnight. A similar synthesis procedure was performed for Pt-MnO_2/CNT. It just changed from Pd solution to Pt solution.

Pt/Pd-MnO_2/CNT

A total of 60 mg of the synthesized MnO_2/CNT composite was dispersed in 15 mL of deionized (DI) water via ultrasonication for 30 min to achieve uniform dispersion. Subsequently, 4 mL of a 10 mM Pd standard solution was added to the suspension. The pH of the mixture was adjusted to approximately 11 using 5 M NaOH. Then, 1 mL of a 0.5 M ascorbic acid (AA) solution was introduced as a reducing agent. The resulting mixture was stirred at room temperature overnight to facilitate the deposition of Pd nanoparticles onto the MnO_2/CNT matrix.

On the following day, 4 mL of a 10 mM Pt standard solution was added to the mixture. The solution was then heated at 90 °C in an oil bath for 1 h to enable the reduction and incorporation of Pt nanoparticles. After cooling to room temperature, the product was washed several times with DI water by centrifugation until a neutral pH was attained. Finally, the precipitate was dried in an oven at 60 °C overnight to obtain the Pt/Pd-MnO_2/CNT nanocomposite powder.

Device fabrication

The synthesized Pt/Pd-MnO_2/CNT nanomaterial was dropped casting on commercial SPE. The modified electrode was then dried in a desiccator overnight at room temperature. Then, the modified SPE is ready for use the following day.

Standard preparation

The conversion of glutamate to H_2O_2 is facilitated by glutamate oxidase. Various glutamate concentrations were prepared, ranging from 5, 20, 40, 60 and 60 µM. For example, to prepare the 20 µM concentration, 20 µL of 100 µM glutamate stock solution was pipetted into an Eppendorf tube, followed by the addition of 10 µL of 0.2 U/mL glutamate oxidase. The volume was then adjusted to 100 µL with PBS buffer to pH 7.4. Subsequently, the resulting mixture was incubated at room temperature for 30 min. After incubation, the production of H_2O_2 was measured using a developed electrochemical sensor. This process was repeated for each concentration of the glutamate standard solution.

Sample preparation

The 0.5 g of instant noodles seasoning powder was weighed and subsequently dissolved in boiling water. After allowing the mixture to cool to room temperature, it was filtered to achieve a homogeneous solution. Subsequently, 1 mL of the filtrate was carefully transferred into a 10 mL volumetric flask and adjusted volume with PBS buffer, pH 7.4. Subsequently, 20 µL of this sample was incubated with 10 µL of 0.2 U/mL glutamate oxidase, and the total volume was adjusted to 100 µL with PBS buffer, pH 7.4. After 30 min of incubation, the produced H_2O_2 was measured using an electrochemical method, and the glutamate concentration was calculated using a calibration method.

Results and discussion

The resulting H_2O_2 from the reaction of glutamate with glutamate oxidase was monitored for glutamate detection, as illustrated in the following equation.

$$\text{Glutamate} + O_2 \xrightarrow[\textit{glutamate oxidase}]{} H_2O_2 + NH_3 + \alpha\text{-ketoglutarate}$$

Characterization

Morphological characterization

The morphology of various screen-printed electrodes (SPEs) was analyzed using SEM, including bare SPE, MnO_2/CNT/SPE, Pd/MnO_2/CNT/SPE, Pt/MnO_2/CNT/SPE, and Pt/Pd-MnO_2/CNT/SPE, as depicted in **Figures 1(a) - 1(e)**. **Figure 1(a)** shows the bare SPE, which exhibits a uniform coverage of carbon material, characteristic of these electrodes. Upon modification with MnO_2/CNT (**Figure 1(b)**), a distinct dispersion of particles is visible, indicating the successful growth and integration of MnO_2 onto the CNT framework. This uniform dispersion suggests a robust interaction and effective coverage of MnO_2 on the CNTs, which is crucial for enhancing the electrochemical properties of the electrode. The MnO_2 functions as a catalyst, while the CNTs provide the conductive support necessary for improved performance.

In the case of Pt-MnO_2/CNT/SPE (**Figure 1(c)**), grain size reduction is likely resulting from the synergistic interaction between MnO_2 and Pt nanoparticles on the CNT surface. This interaction appears to promote a more homogeneous distribution of smaller grains, which increase the active surface area, thereby enhancing the catalytic performance. A similar morphological change is noted for Pd-MnO_2/CNT/SPE (**Figure 1(d)**), suggesting a comparable interaction between Pd and MnO_2 on the CNTs occurs. Furthermore, the SEM image of Pt/Pd-MnO_2/CNT/SPE (**Figure 1(e)**) shows almost complete disappearance of MnO_2 grains, with only small particles dispersed across the electrode surface. This suggests that the Pd and Pt nanoparticles dominate the surface, likely due to a strong interaction that results in the dissolution or significant reduction of MnO_2 grains. The presence of Pd and Pt, known for their high electrocatalytic activities, implies that this composite electrode could provide superior performance in catalytic applications, such as hydrogen peroxide detection. The enhanced dispersion and interaction of the catalytic nanoparticles (Pd and Pt) with MnO_2/CNT are crucial for improving the electrocatalytic properties of the electrodes. These nanoparticles' high surface area and active sites enable efficient electron transfer and catalytic reactions, making Pd/MnO_2/CNT a promising candidate for sensitive and selective H_2O_2 detection.

Further particle size analysis, as shown in **Figures 1(f)** and **1(g)**, is conducted using Transmission Electron Microscopy (TEM), confirming the scale of Pt/Pd-MnO_2/CNT is 50 nm. Additionally, elemental analysis in **Figure 1(h)** reveals that all elements are well-dispersed on the surface of the electrode, with MnO_2, Pt, and Pd materials playing key roles in enhancing electrochemical performance. These materials improve

catalytic activity, which is crucial for efficient electrochemical reactions. The conductive properties of CNTs further support high electron mobility, contributing to the overall efficiency of the electrode. The enhanced dispersion and interaction between the catalytic nanoparticles (Pd and Pt) and MnO_2 on CNT are vital for improving the electrocatalytic properties. These nanoparticles' high surface area and active sites facilitate efficient electron transfer and catalytic reactions, supported by the electrochemical sensing performance shown in **Figure 2**, positioning Pt/Pd-MnO_2/CNT as a promising candidate for sensitive and selective H_2O_2 detection.

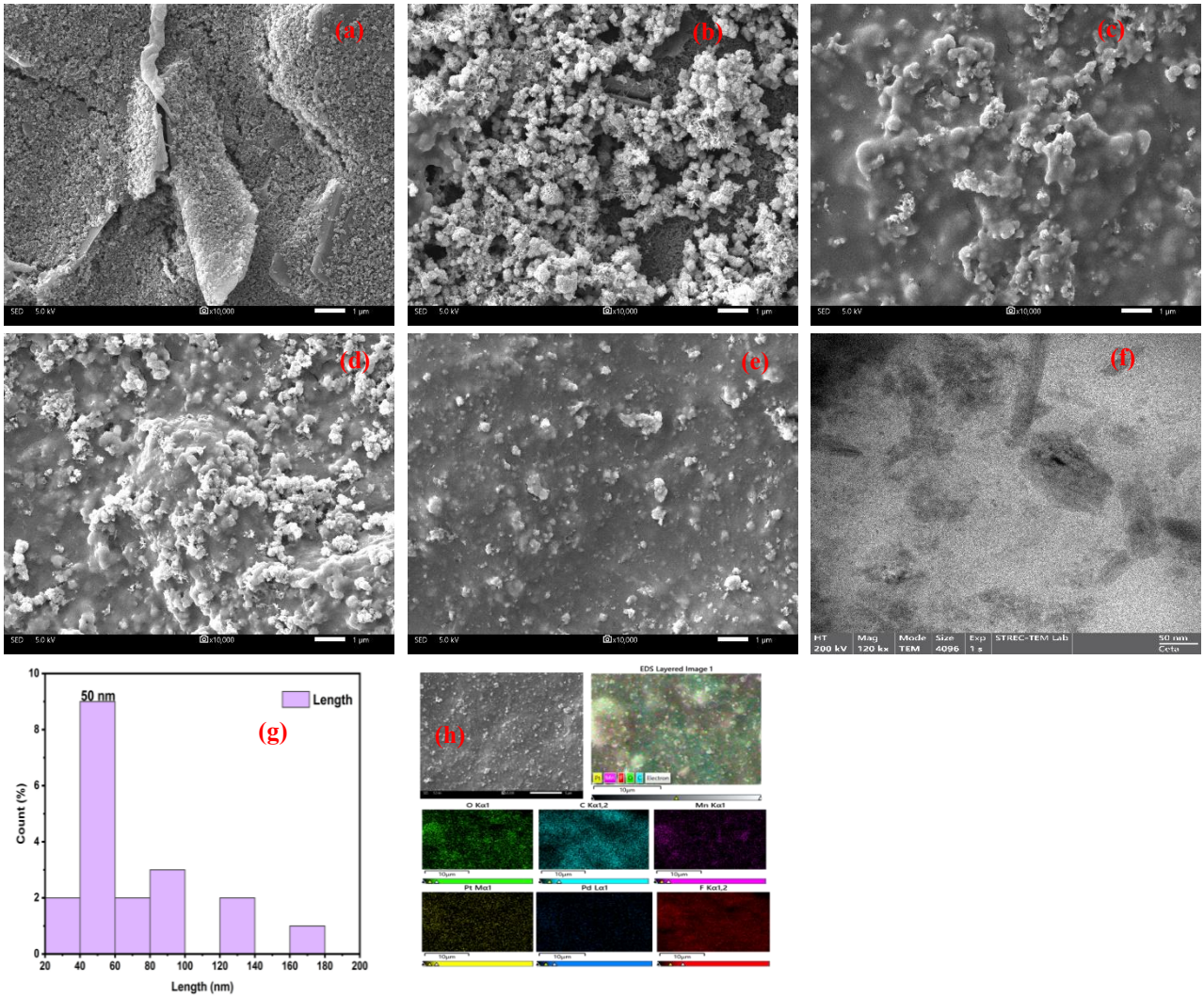

Figure 1 Morphology analysis by SEM (a) bare SPE, (b) MnO_2/CNT, (c) Pd-MnO_2/CNT, (d) Pt- MnO_2/CNT, (e) Pt/Pd-MnO_2/CNT, (f) TEM analysis of Pt/Pd-MnO_2/CNT, particle size analysis (g) and (h) EDS-SEM mapping of Pt/Pd-MnO_2/CNT.

Electrochemical characterization

The electrochemical characteristics of various electrodes, including bare SPE, MnO_2/CNT/SPE, Pd-MnO_2/CNT/SPE, Pt-MnO_2/CNT/SPE, and Pt/Pd-MnO_2/CNT/SPE, were evaluated by measuring the reduction of 1 mM H_2O_2 at a scan rate of 100 mV/s using cyclic voltammetry (CV). **Figure 2** demonstrates that the reduction currents for MnO_2/CNT/SPE, Pd-MnO_2/CNT/SPE, Pt-MnO_2/CNT/SPE, and Pt/Pd-MnO_2/CNT/SPE are higher than that of the bare SPE. This enhancement is attributed to Pd, Pt, MnO_2, and CNT, where Pd, Pt, and MnO_2 contribute electrocatalytic properties, and CNT facilitates conductivity. Compared to the bare SPE, the MnO_2/CNT composite exhibited an increased cathodic current of H_2O_2. Moreover, the introduction of Pd and

Pt into MnO_2/CNT/SPE further amplified its cathodic current, with Pt showing superior catalytic activity compared to Pd, as indicated by the more distinct H_2O_2 reduction peak observed in Pt/MnO_2/CNT/SPE relative to Pd/MnO_2/CNT/SPE. Notably, the combined presence of Pd and Pt within MnO_2/CNT/SPE resulted in a marked increase in the cathodic current for H_2O_2, suggesting a synergistic effect between the 2 metals. This synergy enhances their catalytic efficacy, making the Pt/Pd-MnO_2/CNT/SPE system more effective than metal alone. Therefore, the study highlights the superior electrocatalytic activity of the composite electrodes (MnO_2/CNT/SPE, Pd-MnO_2/CNT/SPE, Pt-MnO_2/CNT/SPE, and Pt/Pd-MnO_2/CNT/SPE) compared to bare SPE. Both Pd and Pt within the MnO_2/CNT/SPE structure led to the most significant improvement in the H_2O_2 cathodic current. This indicates that Pt/Pd-MnO_2/CNT/SPE nanomaterials exhibit enhanced electron transfer capabilities and a synergistic effect, resulting in a substantial increase in the direct electron transfer rate between the target analyte and the electrode. Consequently, the Pt/Pd-MnO_2/CNT/SPE catalyst shows exceptional electrochemical performance in the presence of H_2O_2.

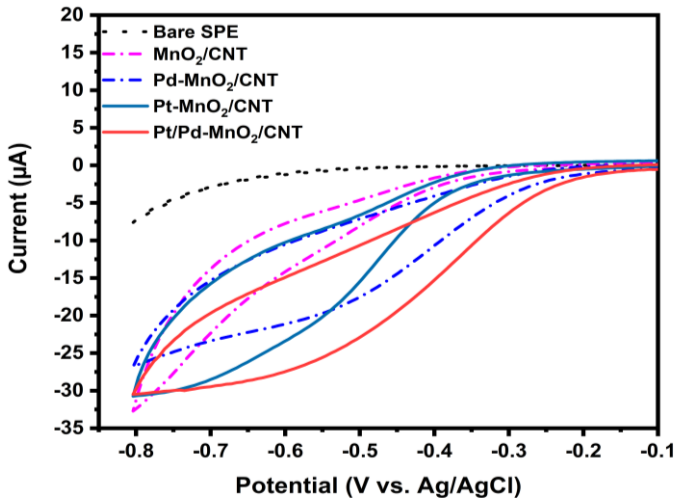

Figure 2 Cyclic voltammograms of 1 mM H_2O_2 in PBS, pH 7.4 at bare SPE, MnO_2/CNT/SPE, Pd-MnO_2/CNT/SPE, Pt-MnO_2/CNT/SPE and Pt/Pd-MnO_2/CNT/SPE at 100 mV/s.

Effect of nanomaterials amount and mass transfer

The impact of nanomaterial thickness on the electrode performance was investigated by varying the amount of Pt/Pd-MnO_2/CNT applied. Different amounts (1, 2, 3 and 4 mg) of nanomaterials were used to evaluate their response to 1 mM H_2O_2 in cyclic voltammetry (CV). As shown in **Figure 3**, an increase in nanomaterial quantity from 1 to 2 mg resulted in a higher reduction of H_2O_2. However, with 3 and 4 mg of nanomaterials, the reduction current of H_2O_2 decreased. This suggests that larger quantities of material correspond to an increase in nanomaterial thickness, which elevates the charging current and hinders the diffusion of the analyte to the electrode surface, ultimately leading to a reduced current. Consequently, 2 mg was selected for further studies.

Additionally, the mass transfer of the H_2O_2 response on the modified electrode was explored by varying scan rates, as shown in **Figures S1(a)** and **S1(b)**. The results demonstrate a consistent increase in the cathodic current of H_2O_2 as the scan rate increased from 10 to 100 mV/s. Furthermore, the linear correlation between the cathodic current of H_2O_2 and the square root of the scan rate, described by the equation I_{pc} (µA) = $-1.3194V^{1/2} - 6.1127$, with a high correlation coefficient (R^2 = 0.9961), indicates a systematic relationship. This linear correlation suggests that the electrocatalytic reduction of H_2O_2 on the Pt/Pd-MnO_2/CNT electrode follows a diffusion-controlled electrochemical reaction.

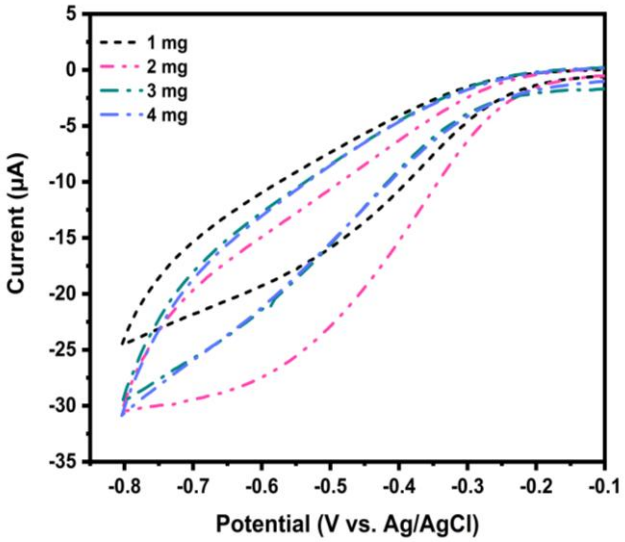

Figure 3 Cyclic voltammograms of 1 mM H_2O_2 in PBS (pH 7.4) recorded at 100 mV/s with Pt/Pd-MnO_2/CNT catalyst loadings of 1, 2, 3 and 4 mg.

Effect of applied potential, and study of repeatability, reproducibility, and stability

The applied potential influences the sensitivity of Pt/Pd-MnO_2/CNT. Current measurements were conducted at various applied potentials to investigate how different potentials affect the current signal of H_2O_2. As shown in **Figure 4(a)**, the current resulting from the electrocatalytic reduction of H_2O_2 gradually increases as the applied potential is raised from −0.1 to −0.6 V. However, beyond this potential, the current remains stable with further increases in applied potential. The most significant ratio of reduction current, as illustrated in **Figure 4(b)** for 1 mM H_2O_2 compared to the buffer, is observed at −0.6 V. Therefore, −0.6 V was selected as the optimal applied potential for subsequent studies.

The consistency of the electrode was evaluated by performing ten measurements of 1 mM H_2O_2 using a single electrode and 10 different electrodes. These measurements were conducted using constant potential testing at −0.6 V with the chronoamperometric technique, as shown in **Figures S2(a)** and **S2(b)**. The results show a favorable relative standard deviation (RSD) of 2.1 % for repeatability (**Figure S2(a)** and 3.03 % for reproducibility (**Figure S2(b)**, demonstrating the electrode's ability to provide consistent and reliable results. Additionally, the stability of the electrode was assessed, as shown in **Figure S2(c)**. After 3 weeks of storage in a desiccator at room temperature, the electrode retained 96 % of its performance, indicating excellent stability.

Specificity and selectivity study

Detecting H_2O_2 is crucial for accurately determining glutamate levels in enzymatic assays, as H_2O_2 is a byproduct of glutamate oxidation facilitated by the enzyme glutamate oxidase. The amount of H_2O_2 produced is directly proportional to the concentration of glutamate in the sample, making it a key parameter for precise glutamate quantification. The detection of H_2O_2 was performed using the chronoamperometric technique.

Ensuring the specificity and selectivity of the sensor is essential for accurate analysis. To verify specificity, the sensor was tested against a range of potential interferents (1 mM), including glutamate (Glu), glucose (G), NaCl, KCl, glycine (Gly), sucrose (Sucr), fructose (Fruc), and 1 mM H_2O_2. As shown in **Figure 5(a)**, these substances produced signals similar to that of the blank (PBS buffer), demonstrating the sensor's specific response to H_2O_2.

Further investigation evaluated the impact of these interferents on H_2O_2 detection. In **Figure 5(b)**, where 1 mM of each interferent was mixed with 1 mM H_2O_2, no significant alteration in the detected H_2O_2 signal was observed. This suggests that the interferences do not

affect H_2O_2 measurement by the sensor at equal concentrations. Moreover, the robustness of the sensor was tested under more challenging conditions, as shown in **Figure S3**, where the concentration of interferents was increased to 10 mM (10-fold higher than 1 mM H_2O_2 concentration). Despite this substantial increase, the H_2O_2 signal remained consistent, indicating the sensor's resilience to high levels of potential interferents.

These findings confirm that the Pt/Pd-MnO_2/CNT sensor exhibits exceptional selectivity and reliability in detecting H_2O_2. Its ability to accurately measure H_2O_2 in the presence of diverse interfering substances highlights its suitability for applications that require precise and interference-free analysis.

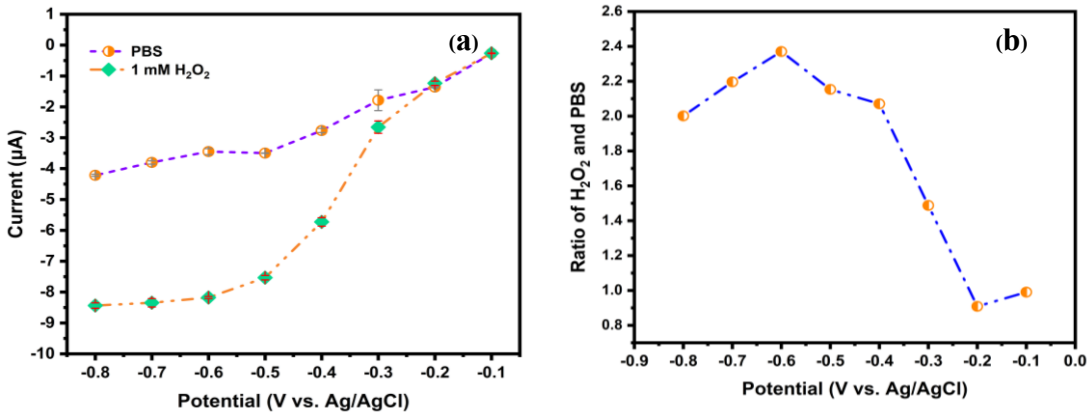

Figure 4 Current responding of (a) applied potential of −0.1, −0.2, −0.3, −0.4, −0.5, −0.6, −0.7 and −0.8 V on 1 mM H_2O_2 and PBS, pH 7.4, (b) ratio between response of 1 mM H_2O_2 and PBS, pH 7.4 at Pt/Pd-MnO_2/CNT/SPE.

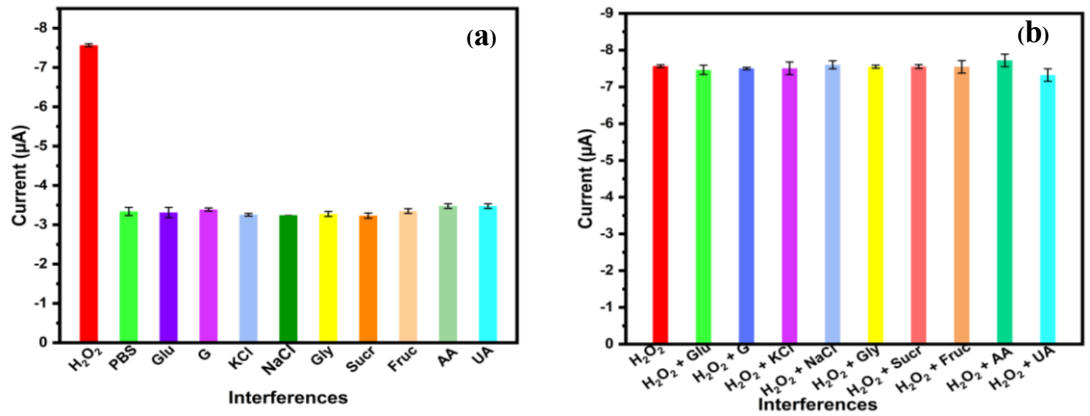

Figure 5 Current responding of (a) interferences study of a sensor developed for measuring 1 mM H_2O_2, and its performance with interference concentrations of (b) 1 mM H_2O_2 mixed 1 mM interferences at Pt/Pd-MnO_2/CNT/SPE at −0.6 V.

Calibration curve

An enzymatic reaction involving glutamate oxidase (GluOx) and glutamate was employed to determine the concentration of glutamate in an actual food sample. This reaction, occurring at a pH of 7.4 and in the presence of oxygen, produces α-ketoglutarate, ammonia, and H_2O_2. The target analyte for measurement is H_2O_2.

Cyclic voltammetry was used to confirm the catalytic conversion of glutamate to H_2O_2. As shown in **Figure S4**, glutamate (0.1 and 1 mM) in PBS saline (pH 7.4) had no redox peaks of any significance, corroborating a lack of electrochemical activity. H_2O_2 (0.1 and 1 mM), on the other hand, showed distinct reduction peaks, demonstrating its electrochemical detectability. In addition, the CV chromatogram of 0.1

and 1 mM glutamate in the presence of GluOx after 30 min reaction with GluOx exhibited a reduction peak similar to that of 0.1 and 1 mM H_2O_2 standard. These results confirm that GluOx successfully converts glutamate to H_2O_2.

In further experiments, Chronoamperometric experiment was performed to construct the calibration curve. Various concentrations of glutamate, ranging from 5 to 80 µM, were tested, as shown in **Figure 6(a)**. The concentration of glutamate oxidase (GluOx) of 0.2 U/mL was used. This enzyme concentration is sufficient for the highest glutamate mole at the maximum concentration in the calibration curve. The current response measured at 150 s was used for quantification. The results revealed a broad linear range with an R^2 value of 0.9985 (**Figure 6(b)**). The limit of detection (LOD) was calculated using the formula 3 times the standard deviation of the blank divided by the slope of the calibration curve. The LOD for detecting glutamate was 1.98 µM.

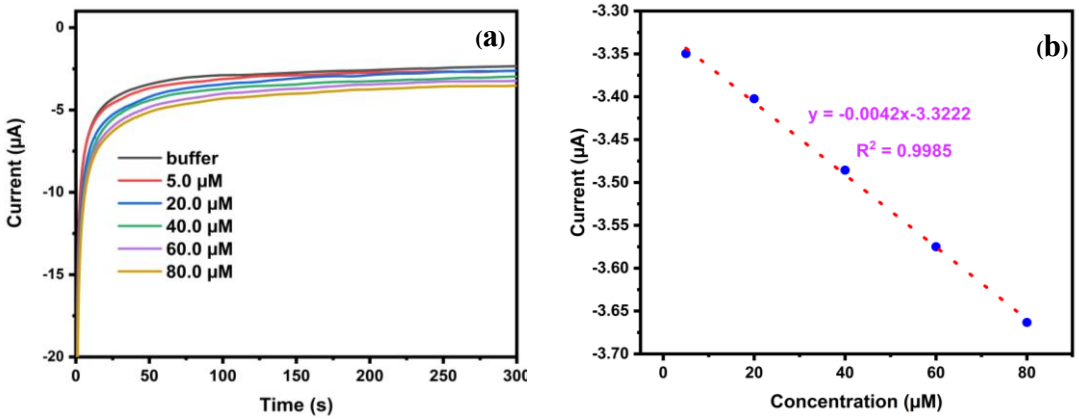

Figure 6 Chronoampergrams of glutamate assay (a), and calibration plot (b) of glutamate at various concentrations from 5 to 80 µM by incubating with 0.2 U/mL glutamate oxidase at Pt/Pd-MnO_2/CNT/SPE at −0.6 V.

Validation method

The validation method was used to confirm the accuracy and precision of the analytical technique. Recovery experiments were conducted by spiking instant noodles seasoning powder (which did not contain monosodium glutamate, MSG) with known concentrations of glutamate standard. Three different concentrations of glutamate standards (20, 40 and 60 µM) were selected based on the linear range of the calibration curve. As shown in **Table 1**, the measured concentrations were 20.90, 39.48 and 60.03 µM, with relative standard deviation (RSD) values of 1.40, 3.03 and 2.06%, respectively. The average recoveries were 105, 99 and 100%, all within the acceptable range. These results demonstrate that the method is precise and accurate for analyzing glutamate in instant noodles seasoning powder.

Table 1 Determination of glutamate spiked in instant noodles seasoning powder using Pt/Pd-MnO_2/CNT/SPE (n = 3).

Instant noodle	Added glutamate (µM)	Found glutamate (µM)	% Recovery
Without MSG	20	20.90 ± 0.30	105
	40	39.48 ± 1.20	99
	60	60.03 ± 1.24	100

Application of developed sensor in seasoning powder of instant noodles

To evaluate the potential of the fabricated sensor for practical analysis, the prepared electrodes were utilized to measure the glutamate concentration in instant noodle seasoning powder. Following the sample preparation procedure outlined in sample preparation step, the chronoamperometric technique was applied under optimal conditions. As shown in **Table 2**, the concentration of glutamate in the seasoning powder was

determined to be 63.55 mg per serving for the Tom Yum flavor, 127.23 mg per serving for the Yentafo Tom Yum Mohfai flavor, and 82.91 mg per serving for the Shrimp Creamy Tom Yum flavor. Additionally, **Table S1** compares key performance indicators - sensitivity, linear range, limit of detection (LOD), and application - of the glutamate detection method developed in this study with other reported techniques. Our method exhibits a notably wider linear detection range for glutamate compared to many previous studies. Furthermore, our sensor enhances catalytic activity and electron transfer efficiency. Unlike previously developed sensors, which suffer from overlapping signals due to AA and UA, our modified electrode structure selectively enhances the cathodic current response to the target analyte while suppressing interference.

Furthermore, it achieves a lower LOD, particularly when compared to reduction-based techniques. The sensor demonstrates excellent selectivity for glutamate, effectively minimizing interference from other substances. Notably, our sensor is fabricated using a simplified and cost-effective approach, enhancing its portability and affordability compared to existing methods. This makes it a promising candidate for practical and accessible glutamate-sensing applications. This approach marks a significant advancement in glutamate detection technology, offering both high performance and practical usability in various applications, including real-time monitoring of food products like instant noodles.

Table 2 Assay of glutamate in the seasoning of instant noodles by the developed sensor.

No.	Seasoning powder of instant noodles	C_{glu} (mg/packet) ± SD) [a] by proposed sensor
1	Shrimp tom yum flavor	63.55 ± 1.55
2	Yentafo tom yum mohfai flavor	127.23 ± 8.93
3	Shrimp creamy tom yum flavor	82.91 ± 2.54

C_{glu} (mg/packet): Glutamate per packet (mg of glutamate per packet of seasoning powder
[a]: Average of 3 replicate

Conclusions

For the first time, we have successfully developed a Pt/Pd-MnO_2/CNT-based nanomaterial for the electrochemical detection of glutamate. The sensor demonstrates a wide glutamate sensing range from 0.005 to 0.08 mM, with a detection limit of 1.98 µM, operating at a low potential of −0.6 V. Additionally, it exhibits high sensitivity, excellent stability, favorable reproducibility and repeatability, and strong anti-interference capability. The developed sensor was successfully applied for quantitatively determining glutamate in instant noodle seasoning, offering superior performance with accurate detection and satisfactory recovery (99 - 105%). The developed sensor was applied to detect glutamate in the seasoning of different types of noodles. The concentration of glutamate was found to be 63.55, 127.23 and 82.91 mg per pocket in the seasoning of Shrimp tom yum flavor, Yentafo tom yum mohfai flavor, and Shrimp creamy tom yum flavor, respectively. This finding suggests that consuming 1 packet of noodles containing 63 mg of glutamate is well within the safe limit for a > 50 kg individual based on the ADI of 30 mg/kg bw/day. However, for children weighing no more than 5 kg, there is a risk of exceeding the acceptable daily intake (ADI) for glutamate if they consume more than 1 packet of instant noodles per day, due to additional glutamate intake from other foods. These results confirm its potential for rapid glutamate detection in complex environments, particularly in food samples. This work presents a promising, low-cost, efficient device for real-world glutamate sensing applications. Furthermore, it provides valuable insights into developing advanced nanomaterials for electrochemical sensor technologies.

Acknowledgements

The authors would like to express their gratitude and acknowledge the Thailand Research Fund, the

Petchra Pra Jom Klao PhD. Research Scholarship, Innovation and Partnerships Office, King Mongkut's University of Technology Thonburi (KMUTT) for providing financial support for this research.

Declaration of Generative AI in Scientific Writing

The authors acknowledge the use of Grammarly in the preparation of this manuscript to improve language and grammar. No content generation or data interpretation was performed by AI. The authors take full responsibility for the content and conclusions of this work.

Credit Author Statement

Chim Math: Conducted experiments, Synthesized nanomaterials, Analysis of the results, and Writing the original manuscript.

Paweenar Duenchay: Provided advice, Suggestions and Revision of the manuscript.

Wijitar Dungchai: Supervision, Investigation, Conceptualization, Methodology, Funding acquisition, and Revision of the manuscript.

References

[1] X Wei, Y Chen, S He, H Lian, X Cao and B Liu. L-histidine-regulated zeolitic imidazolate framework modified electrochemical interface for enantioselective determination of L-glutamate. *Electrochimica Acta* 2021; **400**, 139464.

[2] M Jamal, S Chakrabarty, MA Yousuf, A Khosla and KM Razeeb. Micro and nanostructure based electrochemical sensor platform for glutamate detection. *Microsystem Technologies* 2018; **24**, 4193-4206.

[3] L Yang, R Bai, B Xie, N Zhuang, Z Lv, M Chen, W Dong, J Zhou and M Jiang. A biosensor based on oriented immobilization of an engineered l-glutamate oxidase on a screen-printed microchip for detection of l-glutamate in fermentation processes. *Food Chemistry* 2023; **405**, 134792.

[4] A Mentana, D Nardiello, C Palermo and D Centonze. Accurate glutamate monitoring in foodstuffs by a sensitive and interference-free glutamate oxidase-based disposable amperometric biosensor. *Analytica Chimica Acta* 2020; **1115**, 16-22.

[5] HP Aung and U Pyell. In-capillary derivatization with o-phthalaldehyde in the presence of 3-mercaptopropionic acid for the simultaneous determination of monosodium glutamate, benzoic acid, and sorbic acid in food samples via capillary electrophoresis with ultraviolet detection. *Journal of Chromatography A* 2016; **1449**, 156-165.

[6] W Wang, Y He, Y Gao, H Gao, L Deng, Q Gui, Z Cao, Y Yin and Z Feng. A peptide aptamer based electrochemical amperometric sensor for sensitive L-glutamate detection. *Bioelectrochemistr*y 2022; **146**, 108165.

[7] EFSA Panel on Food Additives and Nutrient Sources added to Food (ANS), A Mortensen, F Aguilar, R Crebelli, A Di Domenico, B Dusemund, MJ Frutos, P Galtier, D Gott, U Gundert-Remy and JC Leblanc. Re-evaluation of glutamic acid (E 620), sodium glutamate (E 621), potassium glutamate (E 622), calcium glutamate (E 623), ammonium glutamate (E 624) and magnesium glutamate (E 625) as food additives. *EFSA Journal* 2017; **15(7)**, e04910.

[8] H Bayomy and E Alamri. Technological and nutritional properties of instant noodles enriched with chickpea or lentil flour. *Journal of King Saud University-Science* 2022; **34(3)**, 101833.

[9] C Farrand, K Charlton, M Crino, J Santos, R Rodriguez-Fernandez, C Ni Mhurchu and J Webster. Know your noodles! assessing variations in sodium content of instant noodles across countries. *Nutrients* 2017; **9(6)**, 612.

[10] F Errington, T Fujikura and D Gewertz. Instant noodles as an antifriction device: Making the BOP with PPP in PNG. *American Anthropologist* 2012; **114(1)**, 19-31.

[11] C Agius, S Von Tucher, B Poppenberger and W Rozhon. Quantification of glutamate and aspartate by ultra-high performance liquid chromatography. *Molecules* 2018; **23(6)**,1389.

[12] AA Monge-Acuña and J Fornaguera-Trías. A high performance liquid chromatography method with electrochemical detection of gamma-aminobutyric acid, glutamate and glutamine in rat brain homogenates. *Journal of Neuroscience Methods* 2009; **183(2)**, 176-181.

[13] ER Moraes, AB Grisolia, KR Oliveira, DL Picanço-Diniz, ME Crespo-López, C Maximino

and AM Herculano. Determination of glutamate uptake by high performance liquid chromatography (HPLC) in preparations of retinal tissue. *Journal of Chromatography. B, Analytical Technologies in the Biomedical and Life Sciences* 2012; **907**, 1-6.

[14] CP Ferreira, FT Antunes, IN Rebelo, CA da Silva Junior, FN Vilanova, DS Corrêa and AH de Souza. Application of the UV-vis spectrophotometry method for the determination of glutamate in the cerebrospinal fluid of rats. *Journal of Pharmaceutical and Biomedical Analysis* 2020; **186**, 113290.

[15] W Khampha, V Meevootisom and S Wiyakrutta. Spectrophotometric enzymatic cycling method using L-glutamate dehydrogenase and D-phenylglycine aminotransferase for determination of L-glutamate in foods. *Analytica Chimica Acta* 2004; **520(1-2)**, 133-139.

[16] CA Vyas, SM Rawls, RB Raffa and JG Shackman. Glutamate and aspartate measurements in individual planaria by rapid capillary electrophoresis. *Journal of Pharmacological and Toxicological Methods* 2011; **63(1)**, 119-122.

[17] JS Marvin, BG Borghuis, L Tian, J Cichon, MT Harnett, J Akerboom, A Gordus, SL Renninger, TW Chen, CI Bargmann and MB Orger. An optimized fluorescent probe for visualizing glutamate neurotransmission. *Nature Methods* 2013; **10(2)**, 162-170.

[18] D Maity and RR Kumar. Highly sensitive amperometric detection of glutamate by glutamic oxidase immobilized Pt nanoparticle decorated multiwalled carbon nanotubes (MWCNTs)/polypyrrole composite. *Biosensors and Bioelectronics* 2019; **130**, 307-314.

[19] L Yu, Q Zhang, D Jin, Q Xu and X Hu. A promising voltammetric biosensor based on glutamate dehydrogenase/Fe_3O_4/graphene/chitosan nanobiocomposite for sensitive ammonium determination in PM 2.5. *Talanta* 2019; **197**, 622-630.

[20] L Luo, F Li, L Zhu, Z Zhang, Y Ding and D Deng. Non-enzymatic hydrogen peroxide sensor based on MnO_2-ordered mesoporous carbon composite modified electrode. *Electrochimica Acta* 2012; **77**, 179-183.

[21] H Lan, L Wang, S Liu, Y Qian, T Jin and L Lu. Highly sensitive electrochemical detection of paracetamol based on MnO_2/MWCNTs-NH_2 composite. *Inorganic Chemistry Communications* 2022; **146**, 110105.

[22] A Meng, X Hong, Y Zhang, W Liu, Z Zhang, L Sheng and Z Li. A free-standing flexible sensor MnO_2-Co/rGO-CNT for effective electrochemical hydrogen peroxide sensing and real-time cancer biomarker assaying. *Ceramics International* 2023; **49(2)**, 2440-2450.

[23] S Chen, Y Xie, X Guo and D Sun. Self-supporting electrochemical sensors for monitoring of cell-released H_2O_2 based on metal nanoparticle/MOF nanozymes. *Microchemical Journal* 2022; **181**, 107715.

[24] J Čović, V Mirceski, A Zarubica, D Enke, S Carstens, A Bojić and M Ranđelović. Palladium-graphene hybrid as an electrocatalyst for hydrogen peroxide reduction. *Applied Surface Science* 2022; **574**, 151633.

[25] S Tajik, H Beitollahi, S Shahsavari and FG Nejad. Simultaneous and selective electrochemical sensing of methotrexate and folic acid in biological fluids and pharmaceutical samples using Fe_3O_4/ppy/Pd nanocomposite modified screen printed graphite electrode. *Chemosphere* 2022; **291**, 132736.

[26] NS Anuar, WJ Basirun, M Shalauddin and S Akhter. A dopamine electrochemical sensor based on a platinum–silver graphene nanocomposite-modified electrode. *RSC Advances* 2020; **10**, 17336-17344.

[27] V Vinoth, N Pugazhenthiran, RV Mangalaraja, A Syed, N Marraiki, H Valdés and S Anandan. Development of an electrochemical enzyme-free glucose sensor based on self-assembled Pt-Pd bimetallic nanosuperlattices. *Analyst* 2020; **145(24)**, 7898-7906.

[28] C Zhang and Z Ma. PtCu nanoprobe-initiated cascade reaction modulated iodide-responsive sensing interface for improved electrochemical immunosensor of neuron-specific enolase. *Biosensors and Bioelectronics* 2019; **143**, 111612.

[29] A Şavk, H Aydın, K Cellat and F Şen. A novel high-performance non-enzymatic electrochemical glucose biosensor based on activated carbon-supported Pt-Ni nanocomposite. *Journal of Molecular Liquids* 2020; **300**, 112355.

[30] R Wu, Y Li, W Gong and PK Shen. One-pot synthesis of Pt-Pd bimetallic nanodendrites with enhanced electrocatalytic activity for oxygen reduction reaction. *ACS Sustainable Chemistry & Engineering* 2019; **7**, 8419-8428.

[31] H Zhang, M Jin and Y Xia. Enhancing the catalytic and electrocatalytic properties of Pt-based catalysts by forming bimetallic nanocrystals with Pd. *Chemical Society Reviews* 2012; **41**, 8035-8049.

[32] GN Vayssilov, Y Lykhach, A Migani, T Staudt, GP Petrova, N Tsud, T Skála, A Bruix, F Illas, KC Prince, V Matolı´n, KM Neyman and J Libuda. Support nanostructure boosts oxygen transfer to catalytically active platinum nanoparticles. *Nature Materials* 2011; **10**, 310-315.

[33] L Lu. Highly sensitive detection of nitrite at a novel electrochemical sensor based on mutually stabilized Pt nanoclusters doped CoO nanohybrid. *Sensors and Actuators B: Chemical* 2019; **281**, 182-190.

[34] X Ru, W Li, X Wang, Z Shi, X Wen, S Mo and D Mo. Regulating the surface local environment of MnO_2 materials via metal-support interaction in Pt/MnO_2 hetero-catalysts for boosting methanol oxidation. *Chemical Engineering Science* 2023; **281**, 119079.

[35] E Kaivosoja, N Tujunen, V Jokinen, V Protopopova, S Heinilehto, J Koskinen and T Laurila. Glutamate detection by amino functionalized tetrahedral amorphous carbon surfaces. *Talanta* 2015; **141**, 175-181.

[36] G Hughes, RM Pemberton, PR Fielden and JP Hart. Development of a novel reagentless, screen-printed amperometric biosensor based on glutamate dehydrogenase and NAD^+, integrated with multi-walled carbon nanotubes for the determination of glutamate in food and clinical applications. *Sensors and Actuators B: Chemical* 2015; **216**, 614-621.

[37] P Salazar, M Martín, RD O'Neill and JL González-Mora. Glutamate microbiosensors based on Prussian Blue modified carbon fiber electrodes for neuroscience applications: *In-vitro* characterization. *Sensors and Actuators B: Chemical* 2016; **235**, 117-125.

[38] X Wang, J Duan, Y Cai, D Liu, X Li, Y Dong and F Hu. A modified nanocomposite biosensor for quantitative l-glutamate detection in beef. *Meat Science* 2020; **168**, 108185.

[39] J Liu, Y Fan, G Chen and Y Liu. Highly sensitive glutamate biosensor based on platinum nanoparticles decorated MXene-Ti_3C_2Tx for l-glutamate determination in foodstuffs. *LWT* 2021; **148**, 111748.

[40] M Marquitan, MD Mark, A Ernst, A Muhs, S Herlitze, A Ruff and W Schuhmann. Glutamate detection at the cellular level by means of polymer/enzyme multilayer modified carbon nanoelectrodes. *Journal of Materials Chemistry B* 2020; **8**, 3631-3639.

[41] F Hu, T Liu, J Pang, Z Chu and W Jin. Facile preparation of porous Co_3O_4 nanocubes for directly screen-printing an ultrasensitive glutamate biosensor microchip. *Sensors and Actuators B: Chemical* 2020; **306**, 127587.

[42] F Teng, S Santhanagopalan, Y Wang and DD Meng. *In-situ* hydrothermal synthesis of 3-dimensional MnO_2-CNT nanocomposites and their electrochemical properties. *Journal of Alloys and Compounds* 2010; **499**, 259-264.

[43] M Wojnicki, K Fitzner and M Luty-Błocho. Kinetic studies of nucleation and growth of palladium nanoparticles. *Journal of Colloid and Interface Science* 2016; **465**, 190-199.